

Model-independent constraints on ultra-light dark matter from the SPARC data

Man Ho Chan, Chu Fai Yeung

Department of Science and Environmental Studies, The Education University of Hong Kong, Hong Kong, China

chanmh@eduhk.hk

ABSTRACT

Ultra-light dark matter (ULDM) is currently one of the most popular classes of cosmological dark matter. The most important advantage is that ULDM with mass $m \sim 10^{-22}$ eV can account for the small-scale problems encountered in the standard cold dark matter (CDM) model like the core-cusp problem, missing satellite problem and the too-big-to-fail problem in galaxies. In this article, we formulate a new simple model-independent analysis using the SPARC data to constrain the range of ULDM mass. In particular, the most stringent constraint comes from the data of a galaxy ESO563-G021, which can conservatively exclude a ULDM mass range $m = (0.14 - 3.11) \times 10^{-22}$ eV. This model-independent excluded range is consistent with many bounds obtained by recent studies and it suggests that the ULDM proposal may not be able to alleviate the small-scale problems.

Subject headings: dark matter

1. Introduction

Observational data of galactic rotation curves and hot gas in galaxy clusters reveal that dark matter exist. Besides, the data from the Cosmic Microwave Background (Planck Collaboration 2020) and the large-scale structure observations (Croft et al. 1999) have also provided a strong evidence for the dark matter existence. Most astrophysicists believe that dark matter consist of unknown particles which almost have no interaction with ordinary matter except gravity. Traditional proposals have suggested some hypothetical massive particles (dark matter mass $m > 10$ MeV) to account for the dark matter. However, null detections of such particles have been obtained in both direct-detection experiments (Aprile et al. 2018)

and large hadron collider experiments (Abecrcrombie et al. 2020). Moreover, a large parameter space of these particles has been ruled out by gamma-ray and radio observations (Ackermann et al. 2015; Chan & Leung 2017; Chan et al. 2019).

Recently, a class of dark matter called ultra-light dark matter (ULDM) has caught more attention. Some early studies have suggested the existence of light scalar or pseudo-scalar particles (Peccei & Quinn 1977; Weinberg 1978). For example, a hypothetical particle called axion can help solve the CP-violation problem of the strong interaction (Peccei & Quinn 1977) and it can be a possible kind of dark matter particle. Various studies show that ULDM particles may have self-interaction to form Bose-Einstein Condensate to mimic large dark matter structures in galaxies (Zhang et al. 2018) or become dark matter superfluid (Berezhiani & Khoury 2016). Moreover, one important advantage is that the ULDM particles with mass $m \sim 10^{-22}$ eV can form small core structures in galaxies with radius \sim kpc and they behave like cold dark matter (CDM) outside the cores (Ferreira 2020). This particular property can simultaneously solve the small-scale problems, including the core-cusp problem (de Blok 2010), the missing satellite problem (Moore et al. 1999) and the too-big-to-fail problem (Boylan-Kolchin, Bullock & Kaplinghat 2011), encountered in the standard CDM model (Ferreira 2020).

Many recent studies have constrained the mass range of ULDM particles using the data of dwarf galaxies. For example, by fitting the observed mass of Sculptor and Fornax dwarf galaxies, the upper limits of ULDM mass are $m_{22} < 1.1$ (Marsh & Pop 2015) and $m_{22} < 0.4$ (González-Morales et al. 2017) respectively, where $m_{22} = m/(10^{-22}$ eV). Also, by fitting the core masses of the Draco and Sextans dwarf galaxies, one can get $m_{22} = 0.8_{-0.3}^{+0.5}$ and $m_{22} = 6_{-2}^{+1}$ (Chen, Schive & Chiueh 2017; Ferreira 2020). Another study considering the Draco II and Triangulum II dwarf galaxies conclude $m_{22} \sim 3.7 - 5.6$ (Calabrese & Spergel 2016). More recent studies using the data of the Milky Way (Maleki, Baghran & Rahvar 2020; Li, Shen & Shive 2020) and high-redshift galaxies (Kulkarni & Ostriker 2020) generally obtain $m_{22} \sim 1$. In view of these constraints, we can see that the possible ranges or limits of ULDM mass are not quite consistent with each other.

In fact, many of these studies are model-dependent and rely on some unjustified assumptions. Generally speaking, constraining the ULDM mass using the central dark matter core properties requires the information of the total dark matter halo mass M_h . The uncertainties of M_h are usually very large and the determination of M_h is somewhat model-dependent. For instance, most studies assume the Navarro-Frenk-White (NFW) profile to describe the ULDM density profile outside the soliton core (Marsh & Pop 2015; Chen, Schive & Chiueh 2017; González-Morales et al. 2017). However, observations of many galaxies seem to suggest an isothermal dark matter profile (or a cored isothermal dark matter profile) rather

than the NFW dark matter profile (Spano et al. 2008; Velander, Kuijken & Schrabback 2011; Grillo 2012). Such a difference would significantly affect the estimated M_h . Also, the cutoff radius of a dark matter halo following the assumption of the NFW or isothermal profile is not very clear. The cutoff radius is usually assumed when the average dark matter density is equal to a certain factor (e.g. 200 times or 500 times) of the cosmological critical density, which may not be justified to precisely define the actual value of M_h . On the other hand, Safarzadeh & Spergel (2020) show that by relaxing the assumption of the slope constraint from classical dwarf galaxies, the allowed mass range would be significantly changed. The slope constraint used also depends on the dark matter profile assumed outside the core. Therefore, many previous conclusions are model-dependent and suffer from a large systematic uncertainty. We need to formulate a less model-dependent framework to give a more robust constraint of ULDM mass.

In this article, we formulate a model-independent method to constrain the ULDM mass range. In this theoretical framework, we only rely on the results of the ULDM numerical simulations without any presumptions of specific dark matter profile or halo mass function. By examining the data of the Spitzer Photometry & Accurate Rotation Curves (SPARC), we discover that the rotation curve data of 5 galaxies can give meaningful and stringent constraints for ULDM. In particular, one of the galaxies ESO563-G021 can conservatively exclude a mass range $m_{22} = 0.14 - 3.11$, which is a crucial range for the ULDM proposal to explain the small-scale problems in the standard CDM model.

2. The theoretical framework

Assume that all dark matter are ULDM particles. Numerical simulations of the ULDM show that the density profile of the innermost central region of the dark matter halos at redshift $z = 0$ follows (Schive et al. 2014; Safarzadeh & Spergel 2020)

$$\rho_{\text{DM}} = \frac{1.9(10m_{22})^{-2}r_c^{-4}}{[1 + 9.1 \times 10^{-2}(r/r_c)^2]^8} 10^9 M_\odot \text{ kpc}^3, \quad (1)$$

where r_c is the core radius at which the density drops to one-half its peak value. Based on this density profile, we can get the enclosed core mass

$$M_c \approx 14 \left(\frac{M_h}{M_\odot} \right)^{1/3} (4.4 \times 10^7 m_{22}^{-3/2})^{2/3} M_\odot, \quad (2)$$

and the core radius

$$r_c \approx 1.6 m_{22}^{-1} \left(\frac{M_h}{10^9 M_\odot} \right)^{-1/3} \text{ kpc} \quad (3)$$

in terms of the ULDM mass m_{22} and the total halo mass M_h (Schive et al. 2014; Safarzadeh & Spergel 2020).

Since $M_h > 10^{10} M_\odot$ for most of the galaxies, if we have $m_{22} \sim 1$, the core radius should be $r_c \sim 1$ kpc. Therefore, by examining the galactic observed data ~ 1 kpc from the galactic centers, we can get a constrained parameter space for m_{22} and M_h . Consider a data point (r_i, M_i) obtained from the rotation curve data of a galaxy, where r_i and M_i are the radius and the enclosed dark matter halo mass at r_i from the galactic center. Since the dark matter halo mass profile $M_{\text{DM}}(r)$ is an increasing function, for $r_i > r_c$, we must have $M_i \geq M_c$. Therefore, it is impossible to have $M_i < M_c$ for $r_i > r_c$. Thus, for a certain parameter space (m_{22}, M_h) such that $M_i < M_c$ and $r_i > r_c$, that parameter space would be the excluded region (see Fig. 1).

In order to get a constrained mass range of m_{22} only, we need to constrain the value of M_h . Calculating the range of M_h is usually model-dependent, like assuming the NFW profile or a certain halo mass function. Nevertheless, we can get a model-independent and conservative lower limit of M_h by analyzing the outermost rotation curve data of a galaxy. For example, if the outermost rotation curve data point of a galaxy gives M_j (the minimum total observed dark matter halo mass), the parameter space of $M_h < M_j$ is excluded. From the parameter space graph (m_{22}, M_h) , if the position of the horizontal line $M_h = M_j$ is higher than the intersection point of the two solid lines (e.g. (m'_{22}, M'_h) in Fig. 1), the excluded regions based on the data (r_i, M_i) and M_j would separate the allowed parameter space of (m_{22}, M_h) into two discrete regions (because the region below the horizontal line $M_j = M_h$ is excluded). The range of m_{22} between the two separated regions would be the excluded m_{22} range.

To get the analytic excluded mass range of m_{22} from the data r_i , M_i and M_j , we can solve Eq. (2) and Eq. (3) directly by putting $M_i = M_c$ and $r_i = r_c$. Therefore, we get

$$M_i = 3.1 \times 10^4 \left(\frac{M_h}{M_\odot} \right)^{1/3} m_{22}^{-1} M_\odot, \quad (4)$$

and

$$r_i = 1600 m_{22}^{-1} \left(\frac{M_h}{M_\odot} \right)^{-1/3} \text{ kpc}. \quad (5)$$

Since $M_h < M_j$ is excluded, we set $M_j = M_h$ to get the excluded m_{22} range. Therefore, the analytic excluded m_{22} range is

$$\frac{1600(M_j/M_\odot)^{-1/3}}{(r_i/1 \text{ kpc})} < m_{22} < \frac{3.1 \times 10^4(M_j/M_\odot)^{1/3}}{(M_i/M_\odot)}. \quad (6)$$

3. Data analysis

We consider the SPARC data in Lelli, McGaugh & Schombert (2016) to constrain m_{22} . The data consist of high-quality rotation curves from 175 nearby galaxies and include four velocity components at different radii r : total rotational velocity V_{tot} , gas disk V_{gas} , stellar disk V_{disk} and bulge V_{bul} (Lelli, McGaugh & Schombert 2016). The total enclosed mass $M(r) = rV_{\text{tot}}^2/G$ is a sum of the enclosed dark matter halo mass $M_{\text{DM}}(r)$ and the baryonic mass $M_{\text{bar}}(r)$. Therefore, the dark matter halo mass can be obtained by (Lelli, McGaugh & Schombert 2016)

$$M_{\text{DM}}(r) = \frac{r}{G} [V_{\text{tot}}^2 - |V_{\text{gas}}|V_{\text{gas}} - \Upsilon_{\text{disk}}|V_{\text{disk}}|V_{\text{disk}} - \Upsilon_{\text{bul}}|V_{\text{bul}}|V_{\text{bul}}], \quad (7)$$

where Υ_{disk} and Υ_{bul} are the stellar mass-to-light ratios for the disk and bulge components respectively. By examining the first few data points (i.e. at small radii r) and using Eq. (7), we can obtain the data points (r_i, M_i) for different galaxies. However, the actual values of Υ_{disk} and Υ_{bul} are not very well-known for different galaxies. To make a conservative calculations (i.e. maximizing the M_{DM}), we take $\Upsilon_{\text{disk}} = \Upsilon_{\text{bul}} = 0$ so that we get the possible maximum dark matter halo mass $M_{\text{DM,max}}(r_i) = r_i(V_{\text{tot}}^2 - V_{\text{gas}}|V_{\text{gas}}|)/G \equiv M_i$ for different galaxies.

On the other hand, we need to calculate the minimum total dark matter halo mass M_h for conservative calculations. We select the outermost rotation curve data point (at r_j) for each galaxy and use Eq. (7) to calculate $M_j \equiv M_{\text{DM}}(r_j)$. Since the bulge component is nearly negligible at the outermost region of a galaxy, we can safely assume $\Upsilon_{\text{bul}} = 0$. For the disk component, we take the conservative maximum value $\Upsilon_{\text{disk}} = 0.7$ (Lelli, McGaugh & Schombert 2016) to obtain the minimum total dark matter halo mass $M_{\text{DM,min}}(r_j) = M_j$ for our standard analysis. Generally speaking, increasing the value of the maximum Υ_{disk} would give less stringent constraints for m_{22} . Beside the conservative value of $\Upsilon_{\text{disk}} = 0.7$, we will also obtain the limits of m_{22} for different possible values of Υ_{disk} .

After checking with the data of the whole SPARC sample, we find that there are five galaxies (DDO161, ESO563-G021, IC4202, NGC1090, NGC6015) which have appropriate (r_i, M_i) and M_j that can separate the allowed parameter space of (m_{22}, M_h) into two discrete regions. By using the analytic formula in Eq. (6), we can get the excluded range of m_{22} for each galaxy. The corresponding data and the excluded ranges of m_{22} are shown in Table 1. In fact, the observed values of the total rotational velocity for each galaxy have the 1σ error bars ΔV_{tot} . The errors mainly come from the fitting procedures and the errors due to considering of the approaching and receding sides of the disk (Lelli, McGaugh & Schombert 2016). In our analysis, we have included the corresponding 1σ limit for each data point in determining the values of M_i and M_j (i.e. using the values of $V_{\text{tot}} + \Delta V_{\text{tot}}$ to determine M_i

and $V_{\text{tot}} - \Delta V_{\text{tot}}$ to determine M_j). Moreover, note that the gas velocities can be negative in the innermost regions because the gas distribution may have a significant central depression and the material in the outer regions could exert a stronger gravitational force than that in the inner parts (Lelli, McGaugh & Schombert 2016). In our five sample galaxies, both NGC1090 and NGC6015 have a negative velocity gas component in the innermost regions. We have considered this factor in our analysis, although the overall effect of the negative velocity gas component in these two galaxies is about 1% only. Since the data points in Lelli, McGaugh & Schombert (2016) are continuous in r , we can combine the excluded ranges of m_{22} obtained from the same galaxy and get the overall excluded ranges. Among the results in Table 1, the constraints obtained by the ESO563-G021 galaxy are the most stringent. The excluded mass range $m_{22} = 0.14 - 3.11$ basically covers the excluded ranges based on the other four galaxies.

In Fig. 2, we show the graphical analysis of the data from the ESO563-G021 galaxy. There are two data points (r_i, M_i) which can separate the allowed m_{22} into two discrete regions (i.e. two pairs of lines are plotted). It has a relatively large minimum total dark matter halo mass M_j so that the excluded range (shaded region) is somewhat wider. We also show the similar graphical analyses for the other four galaxies in Fig. 3. If we assume a larger value of Υ_{disk} , the value of M_j for each galaxy would decrease and the corresponding limits would be less stringent. We show the corresponding excluded ranges of m_{22} for three other values of Υ_{disk} in Table 2.

Note that some inner regions (≤ 0.5 kpc) of our target galaxies are considered in our analysis. In such inner regions, the radial velocity component (or radial velocity dispersion) v_r may dominate the velocity of the dark matter tracer’s orbit so that the total enclosed mass calculated by the rotational speed may not be correct. Nevertheless, except the IC4202 galaxy, the other four galaxies do not have any spherical bulge component. Therefore, the effect of v_r would be smaller in these four galaxies. In fact, the effect of the radial velocity component can be characterized by the anisotropy parameter $\beta = 1 - (v_t/v_r)^2$, where v_t is the tangential velocity component. From the Jeans equation, the total enclosed mass is $M(r) = rv_r^2(\gamma_* + \gamma_r - 2\beta)/G$, where γ_* and γ_r are the gradient of the stellar mass distribution and the gradient of v_r respectively (Wolf et al. 2010). For the bulgeless galaxies at small $r \leq 0.5$ kpc, the disk components with disk scale radius $r_d \sim 5 - 10$ kpc dominate the stellar distribution. For the region $r/r_d \leq 0.1$, the disk stellar density is almost constant so that the stellar density gradient $\gamma_* \sim r/r_d$ and the value of γ_r are relatively small. Therefore, the value of $M(r)$ is dominated by the term $2r(v_t^2 - v_r^2)/G$. However, the contribution of the v_r component is negative, which would give a smaller total enclosed mass. As a result, the enclosed dark matter halo mass calculated based on our data without considering the v_r component would be overestimated so that the excluded m_{22} ranges obtained are more

conservative. Nevertheless, the effect of v_r in IC4202 galaxy may be relatively larger because it has a bulge component which may have a larger value of γ_* at small r .

4. Discussion

In this article, we have described a new and simple model-independent analysis to constrain m_{22} . We can write the excluded mass range of m_{22} analytically in terms of the data of galactic rotation curves r_i , M_i and M_j . Using the SPARC data, we find that there are five galaxies which can give stringent constraints for m_{22} . Note that besides the five chosen galaxies, all the remaining galaxies in the SPARC sample cannot give any meaningful constraints based on our method because $M_j \leq M'_h$ in these galaxies. In other words, the total enclosed mass content manifested by the outermost data in these galaxies is not large enough to give any useful limits (i.e. no excluded ranges of m_{22} can be obtained).

The overall excluded mass range is $m_{22} = 0.14 - 3.11$ in our standard analysis, assuming a conservative upper limit of $\Upsilon_{\text{disk}} = 0.7$. This excluded mass range is conservative as we have maximized the possible dark matter halo mass at small r by setting $\Upsilon_{\text{disk}} = \Upsilon_{\text{bul}} = 0$ and minimized the possible total dark matter halo mass M_h at large r by putting a maximum value of $\Upsilon_{\text{disk}} = 0.7$. The actual excluded mass range should be larger as the actual value of M_h is larger than the value of M_j in these galaxies. Moreover, the dark matter halo mass is directly probed from the rotation curves, which does not have any presumption of specific dark matter density profile. The only assumption made in this analysis is the density core formed based on the numerical simulations (i.e. Eq. (1)).

In fact, the gravity and the baryonic feedback of the baryonic components may have significant impact on the resultant dark matter density profile. Recent numerical simulations involving baryons have examined how baryons affect the dark matter density core formed (Mocz et al. 2019; Veltmaat, Schwabe & Niemeyer 2020). In particular, Mocz et al. (2019) show that the dark matter structure at early times is largely unaffected by the effects of baryonic feedback and reionization. On the other hand, a more recent study shows that the dark matter core formed by the ULDM with baryons has a higher core density than that of the ULDM-only simulations at redshift $z = 4.0$ (Veltmaat, Schwabe & Niemeyer 2020). If it is also true for $z = 0$, this result would give a much tighter constraint for the upper limit of m_{22} because it would give a larger M_c in general. Therefore, our constraints based on the ULDM-only simulations would be more conservative. Besides the baryonic effects, the non-linear dynamical effects of the large-volume cosmological simulations on the ULDM density profile might also be important. However, due to the limited resolution, the effect is still uncertain and further investigations are required to understand the actual effect (May & Springel

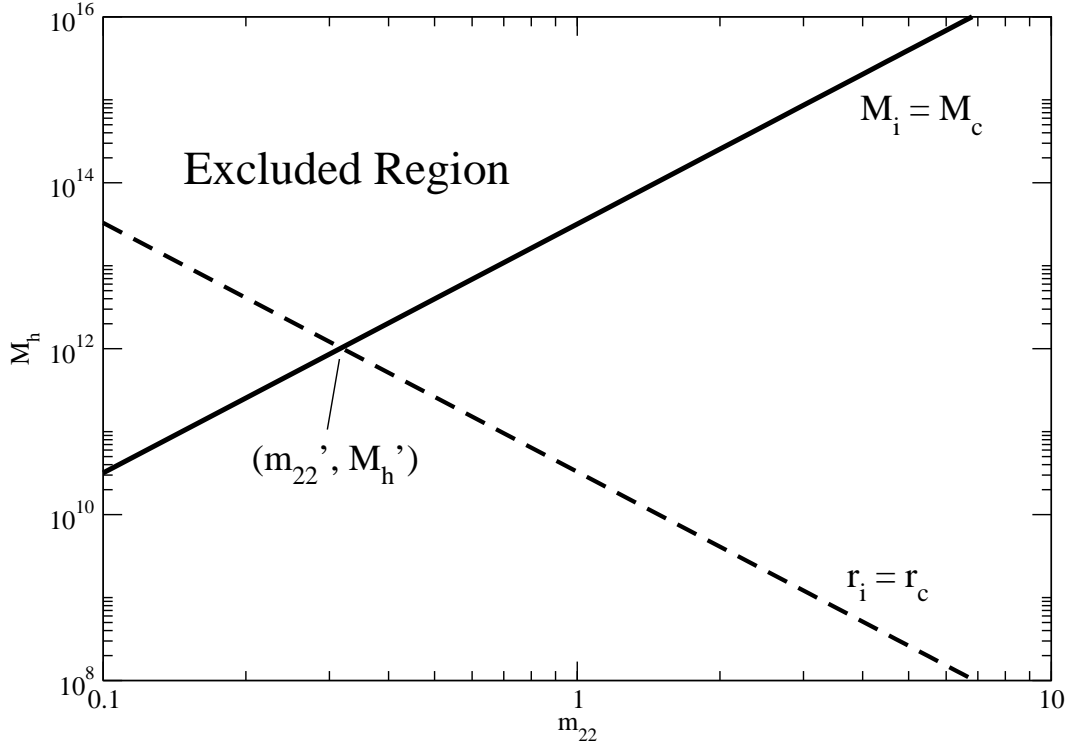


Fig. 1.— The solid and dashed lines represent the relations $M_i = M_c$ and $r_i = r_c$ respectively. Here, we arbitrary set $M_i = 10^9 M_\odot$ and $r_c = 0.5$ kpc for illustration. The upper region bounded by the solid and dashed lines is the excluded parameter space of (m_{22}, M_h) . The (m'_{22}, M'_h) is the intersection point of the solid and dashed lines. The unit for M_h is in solar mass.

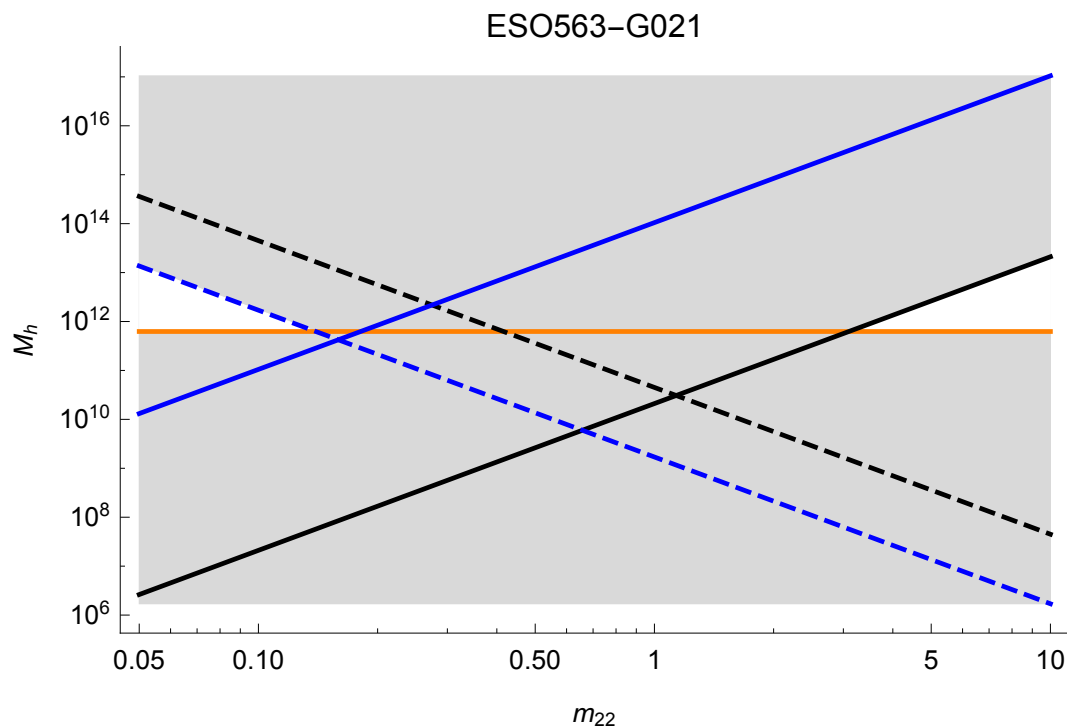


Fig. 2.— The blue and black solid lines represent the relation $M_i = M_c$ (two data points) while the blue and black dashed lines represent the relation $r_i = r_c$ (two data points) for the ESO563-G021 galaxy. The orange solid horizontal line represents the lower limit of $M_h = M_j$ (assuming $\Upsilon_{\text{disk}} = 0.7$). The gray region is the excluded parameter space of (m_{22}, M_h) . The unit for M_h is in solar mass.

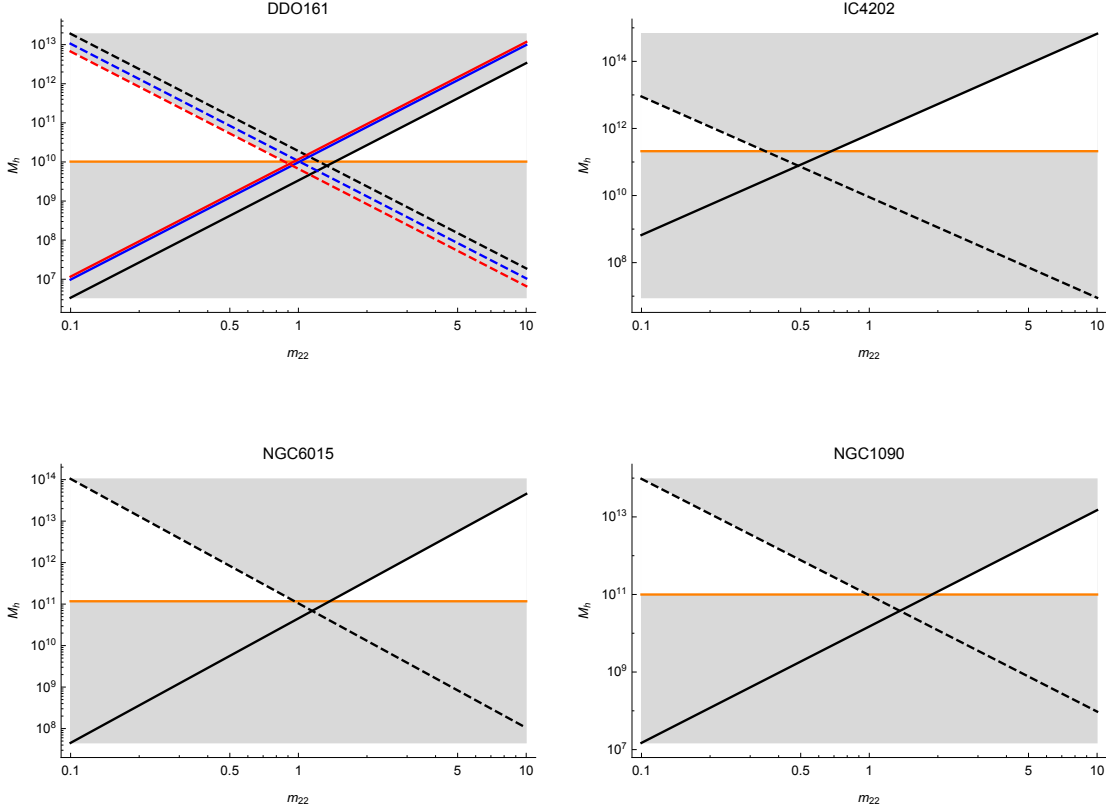


Fig. 3.— The blue, red and black solid lines represent the relation $M_i = M_c$ while the blue, red and black dashed lines represent the relation $r_i = r_c$ for four other galaxies DDO161, IC4202, NGC6015 and NGC1090 (there are three data points for DDO161 galaxy). The orange solid horizontal lines represent the lower limits of $M_h = M_j$ (assuming $\Upsilon_{\text{disk}} = 0.7$). The gray regions are the excluded parameter space of (m_{22}, M_h) . The unit for M_h is in solar mass.

2021). Moreover, although numerical simulations show that the dark matter density behaves like the NFW profile in the outer region (Schive et al. 2014), we do not assume any specific dark matter density profile in our analysis because the baryonic effects have not been precisely considered in the numerical simulations. We have probed the dark matter halo profiles from the observed rotation curves, which are model-independent and more reliable.

The most important feature of the ULDM model is that it can explain the core-like structures in galaxies and behave like CDM outside the central core region if $m_{22} \sim 1$ (Ferreira 2020). Furthermore, it can also address the missing satellite problem and the too-big-to-fail problem (Ferreira 2020). Therefore, the ULDM model with $m_{22} \sim 1$ can simultaneously solve the small-scale problems encountered by the CDM model and agree with the large-scale properties manifested by the CDM model (e.g. Ly α spectrum). However, the conservative excluded mass range $m_{22} = 0.14 - 3.11$ obtained from our analysis has covered a crucial mass range that would significantly challenge the biggest advantage of the ULDM model. If $m_{22} \geq 3.11$, then the Jeans mass (minimum mass of substructure created) would be $\leq 10^7 M_\odot$, which means that halos with mass $\sim 10^7 - 10^8$ are still highly created. Therefore, the missing satellite problem and the too-big-to-fail problem would not be alleviated. Also, for a normal dark matter halo mass $M_h \geq 10^{10} M_\odot$, the core size would be less than 0.25 kpc if $m_{22} \geq 3.11$. Such a core size would be too small to account for the observed size, which may range from $\sim 0.3 - 10$ kpc (Burkert 2020). Also, Burkert (2020) has recently suggested that the fuzzy dark matter model (a kind of ULDM model) cannot account for the core formation in galaxies because the observed constant column density for galaxies is in disagreement with the ULDM simulation prediction. Therefore, our results seem to be consistent with this suggestion and would further wash out this most important advantage of the ULDM model. Nevertheless, the small-scale problems can still be explained by other possible mechanisms, such as dark matter self-interaction (Spergel & Steinhardt 2000; Chan 2013) and baryonic feedbacks (Pontzen & Governato 2014).

Generally speaking, our results are consistent with some recent bounds obtained. For example, Safarzadeh & Spergel (2020) suggest that m_{22} should be larger than 6 if the slope constraints from classical dwarf galaxies are relaxed. Also, using the data of the Milky Way galaxy, Maleki, Baghran & Rahvar (2020) and Li, Shen & Shive (2020) suggest $m_{22} = 25_{-20}^{+36}$ and $m_{22} \sim 2 - 7$ respectively. Further investigation might put focus on $m_{22} > 3$ or $0.01 \leq m_{22} \leq 0.1$ as Cosmic Microwave Background data generally allow $m_{22} \geq 0.01$ (Hlozek et al. 2015). However, these ranges of m_{22} would not be able to alleviate the small-scale problems of the CDM model.

The work described in this paper was partially supported by a grant from the Research Grants Council of the Hong Kong Special Administrative Region, China (Project No.

Table 1: The data derived from the observed rotation curves in Lelli, McGaugh & Schombert (2016) and the corresponding excluded mass ranges for the five galaxies (assuming $\Upsilon_{\text{disk}} = 0.7$).

Galaxy	$M_j (M_{\odot})$	r_i (kpc)	$M_i (M_{\odot})$	excluded m_{22}
DDO161	1.02×10^{10}	0.60	4.67×10^7	1.23-1.46
		0.73	6.67×10^7	1.01-1.02
		0.85	7.09×10^7	0.87-0.96
ESO563-G021	6.25×10^{11}	0.45	8.60×10^7	0.42-3.11
		1.34	1.47×10^9	0.14-0.18
IC4202	2.10×10^{11}	0.77	2.72×10^8	0.35-0.68
NGC1090	9.97×10^{10}	0.35	7.67×10^7	0.99-1.89
NGC6015	1.17×10^{11}	0.34	1.11×10^8	0.96-1.36

Table 2: The excluded ranges of m_{22} for the five galaxies with different Υ_{disk} .

Galaxy	$\Upsilon_{\text{disk}} = 0.7$	$\Upsilon_{\text{disk}} = 0.9$	$\Upsilon_{\text{disk}} = 1.1$	$\Upsilon_{\text{disk}} = 1.3$
DDO161	0.87-1.46	0.87-1.45	0.87-1.45	0.88-1.44
ESO563-G021	0.14-3.11	0.15-2.99	0.15-2.86	0.16-2.72
IC4202	0.35-0.68	0.37-0.65	0.40-0.60	0.44-0.55
NGC1090	0.99-1.89	1.05-1.79	1.12-1.67	1.22-1.53
NGC6015	0.96-1.36	0.98-1.34	1.00-1.31	1.02-1.28

EdUHK 28300518).

REFERENCES

- Abecrcrombie D. *et al.*, 2020, *Phys. Dark Univ.* 27, 100371.
- Ackermann M. *et al.*, 2015, *Phys. Rev. Lett.* 115, 231301.
- Aprile E. *et al.*, 2018, *Phys. Rev. Lett.* 121, 111302.
- Berezhiani L. & Khoury J., 2016, *Phys. Lett. B* 753, 639.
- Boylan-Kolchin M., Bullock J. S. & Kaplinghat M., 2011, *Mon. Not. R. Astron. Soc.* 415, L40.
- Burkert A., 2020, *Astrophys. J.* 904, 161.
- Calabrese E. & Spergel D. N., 2016, *Mon. Not. R. Astron. Soc.* 460, 4397.
- Chan M. H., 2013, *Mon. Not. R. Astron. Soc.* 433, 2310.
- Chan M. H. & Leung C. H., 2017, *Sci. Rept.* 7, 14895.
- Chan M. H., Cui L., Liu J. & Leung C. S., 2019, *Astrophys. J.* 872, 177.
- Chen S.-R., Schive H.-Y. & Chiueh T., 2017, *Mon. Not. R. Astron. Soc.* 468, 1338.
- Croft R. A. C., Weinberg D. H., Pettini M., Hernquist L. & Katz N., 1999, *Astrophys. J.* 520, 1.
- de Blok W. J. G., 2010, *Adv. Astron.* 2010, 789293.
- Ferreira E. G. M., arXiv:2005.03254.
- González-Morales A. X., Marsh D. J. E., Peñarrubia J. & Ureña-López L. A., 2017, *Mon. Not. R. Astron. Soc.* 472, 1346.
- Grillo C., 2012, *Astrophys. J.* 747, L15.
- Hlozek R., Grin D., Marsh D. J. E. & Ferreira P. G., 2015, *Phys. Rev. D* 91, 103512.
- Kulkarni M. & Ostriker J. P., arXiv:2011.02116.
- Lelli F., McGaugh S. S. & Schombert J. M., 2016, *Astron. J.* 152, 157.

- Li Z., Shen J. & Schive H.-Y., 2020, *Astrophys. J.* 889, 88.
- Maleki A., Baghran S. & Rahvar S., 2020, *Phys. Rev. D* 101, 103504.
- Marsh D. J. E. & Pop A.-R., 2015, *Mon. Not. R. Astron. Soc.* 451, 2479.
- May S. & Springel V., 2021, arXiv:2101.01828.
- Mocz P. *et al.*, 2019, *Phys. Rev. Lett.* 123, 141301.
- Moore B. *et al.*, 1999, *Astrophys. J.* 524, L19.
- Peccei R. D. & Quinn H. R., 1977, *Phys. Rev. Lett.* 38, 1440.
- Planck Collaboration Aghanim N. *et al.*, 2020, *Astron. Astrophys.* 641, A6.
- Pontzen A. & Governato F., 2014, *Nature* 506, 171.
- Safarzadeh M. & Spergel D. N., 2020, *Astrophys. J.* 893, 21.
- Schive H.-Y., Liao M.-H., Woo T.-P., Wong S.-K., Chiueh T., Broadhurst T. & Hwang W.-Y. P., 2014, *Phys. Rev. Lett.* 113, 1290.
- Spano M., Marcellin M., Amram P., Carignan C., Epinat B. & Hernandez O., 2008, *Mon. Not. R. Astron. Soc.* 383, 297.
- Spergel D. N. & Steinhardt P. J., 2000, *Phys. Rev. Lett.* 84, 3760.
- Velander M., Kuijken K. & Schrabback T., 2011, *Mon. Not. R. Astron. Soc.* 412, 2665.
- Veltmaat J., Schwabe B. & Niemeyer J. C., 2020, *Phys. Rev. D* 101, 083518.
- Weinberg S., 1978, *Phys. Rev. Lett.* 40, 223.
- Wolf J., Martinez G. D., Bullock J. S., Kaplinghat M., Geha M., Munoz R. R., Simon J. D. & Avedo F. F., 2010, *Mon. Not. R. Astron. Soc.* 406, 1220.
- Zhang X., Chan M. H., Harko T., Liang S.-D. & Leung C. S., 2018, *Eur. Phys. J. C*, 78, 346.